

Structure, ferroelectric, and enhanced fatigue properties of sol-gel-processed new Bi-based perovskite thin films of $Bi(Cu_{1}/_{2}Ti1/_{2})O_3$-$PbTiO_3$

Wei-Bin Song(宋伟宾), Guo-Qiang Xi(席国强), Zhao Pan(潘昭), Jin Liu(刘锦), Xu-Bin Ye(叶旭斌), Zhe-Hong Liu(刘哲宏), Xiao Wang(王潇), Peng-Fei Shan(单鹏飞), Lin-Xing Zhang(张林兴), Nian-Peng Lu(鲁年鹏), Long-Long Fan(樊龙龙), Xiao-Mei Qin(秦晓梅), and You-Wen Long(龙有文)

Citation: Chin. Phys. B, 2024, 33 (**5**): 057701. DOI: 10.1088/1674-1056/ad2a71
Journal homepage: http://cpb.iphy.ac.cn; http://iopscience.iop.org/cpb

What follows is a list of articles you may be interested in

$BaTiO_3$/p-GaN/Au self-driven UV photodetector with bipolar photocurrent controlled by ferroelectric polarization

Wushuang Han(韩无双), Kewei Liu(刘可为), Jialin Yang(杨佳霖), Yongxue Zhu(朱勇学), Zhen Cheng(程祯), Xing Chen(陈星), Binghui Li(李炳辉), Lei Liu(刘雷), and Dezhen Shen(申德振)
Chin. Phys. B, 2024, 33 (**4**): 047701. DOI: 10.1088/1674-1056/ad2607

Impact of annealing temperature on the ferroelectric properties of $W/Hf_{0.5}Zr_{0.5}O_2/W$ capacitor

Dao Wang(王岛), Yan Zhang(张岩), Yongbin Guo(郭永斌), Zhenzhen Shang(尚真真), Fangjian Fu(符方健), and Xubing Lu(陆旭兵)
Chin. Phys. B, 2023, 32 (**9**): 097701. DOI: 10.1088/1674-1056/aca9c6

Charge trapping effect at the interface of ferroelectric/interlayer in the ferroelectric field effect transistor gate stack

Xiaoqing Sun(孙晓清), Hao Xu(徐昊), Junshuai Chai(柴俊帅), Xiaolei Wang(王晓磊), and Wenwu Wang(王文武)
Chin. Phys. B, 2023, 32 (**8**): 087701. DOI: 10.1088/1674-1056/acd524

Domain size and charge defects affecting the polarization switching of antiferroelectric domains

Jinghao Zhu(朱静浩), Zhen Liu(刘震), Boyi Zhong(钟柏仪), Yaojin Wang(汪尧进), and Baixiang Xu(胥柏香)
Chin. Phys. B, 2023, 32 (**4**): 047701. DOI: 10.1088/1674-1056/aca39e

Ferroelectricity induced by the absorption of water molecules on double helix SnIP

Dan Liu(刘聃), Ran Wei(魏冉), Lin Han(韩琳), Chen Zhu(朱琛), and Shuai Dong(董帅)
Chin. Phys. B, 2023, 32 (**3**): 037701. DOI: 10.1088/1674-1056/ac7f8e

---

Structure, ferroelectric, and enhanced fatigue properties of sol–gel-processed new Bi-based perovskite thin films of $Bi(Cu_{1/2}Ti_{1/2})O_3$–$PbTiO_3$

Wei-Bin Song(宋伟宾)[1,2], Guo-Qiang Xi(席国强)[3], Zhao Pan(潘昭)[2,†], Jin Liu(刘锦)[2], Xu-Bin Ye(叶旭斌)[2], Zhe-Hong Liu(刘哲宏)[2], Xiao Wang(王潇)[2], Peng-Fei Shan(单鹏飞)[2], Lin-Xing Zhang(张林兴)[3], Nian-Peng Lu(鲁年鹏)[2,4], Long-Long Fan(樊龙龙)[5], Xiao-Mei Qin(秦晓梅)[1,‡], and You-Wen Long(龙有文)[2,4,§]

[1] *Department of Physics, Shanghai Normal University, Shanghai* 200234, *China*
[2] *Beijing National Laboratory for Condensed Matter Physics, Institute of Physics, Chinese Academy of Sciences, Beijing* 100190, *China*
[3] *Institute for Advanced Materials Technology, University of Science and Technology Beijing, Beijing* 100083, *China*
[4] *Songshan Lake Materials Laboratory, Dongguan* 523808, *China*
[5] *Institute of High Energy Physics, Chinese Academy of Sciences, Beijing* 100049, *China*

(Received 12 December 2023; revised manuscript received 4 February 2024; accepted manuscript online 19 February 2024)

Bi-based perovskite ferroelectric thin films have wide applications in electronic devices due to their excellent ferroelectric properties. New Bi-based perovskite thin films $Bi(Cu_{1/2}Ti_{1/2})O_3$–$PbTiO_3$ (BCT–PT) are deposited on $Pt(111)/Ti/SiO_2/Si$ substrates in the present study by the traditional sol–gel method. Their structures and related ferroelectric and fatigue characteristics are studied in-depth. The BCT–PT thin films exhibit good crystallization within the phase-pure perovskite structure, besides, they have a predominant (100) orientation together with a dense and homogeneous microstructure. The remnant polarization ($2P_r$) values at 30 μC/cm^2 and 16 μC/cm^2 are observed in 0.1BCT–0.9PT and 0.2BCT–0.8PT thin films, respectively. More intriguingly, although the polarization values are not so high, 0.2BCT–0.8PT thin films show outstanding polarization fatigue properties, with a high switchable polarization of 93.6% of the starting values after 10^8 cycles, indicating promising applications in ferroelectric memories.

Keywords: ferroelectric, thin films, perovskite, $PbTiO_3$–BiMeO$_3$

PACS: 77.84.–s, 73.90.+f, 77.84.Cg, 77.84.Cg **DOI:** 10.1088/1674-1056/ad2a71

1. Introduction

The perovskite-structured (ABO_3) ferroelectric thin films, including the typical lead zirconate titanate ($Pb(Zr_{1-x}Ti_x)O_3$, PZT), have been widely investigated recently in terms of their possible applications in microelectro-mechanical systems (MEMS), nonvolatile ferroelectric random access memories (FeRAM), and high-power electric systems because of the high ferroelectric performances and good temperature stabilities.[1–3] However, low Curie temperature ($T_C = 386$ °C) for commercial PZT motivates us to explore novel ferroelectric materials that possess favorable temperature stabilities and T_C values.[4]

Since the superb piezoelectric characteristics in $(1-x)PbTiO_3$–$xBiScO_3$ (PT–BS) surrounding morphotropic phase boundary (MPB) ($x = 0.64$, $d_{33} = 460$ pC/N, and $T_C = 450$ °C) was discovered,[5] the attention of the search for high-T_C as well as favorable temperature stability ferroelectric materials have been paid to the general BiMeO$_3$–$PbTiO_3$ systems, where Me is the single cation or cation mixture, with mean valence being +3). Both experimental and first-principles calculations have proposed that Bi^{3+} with a similar stereochemical $6s^2$ lone-pair electrons to that of Pb^{2+} plays an essential role in enhancing T_C and ferroelectricity.[6,7] Note that PT–BS thin films have been proved to have good piezoelectric and ferroelectric characteristics.[8] Nonetheless, PT–BS application has been greatly limited due to the expensive Sc. Therefore, many researches have focused on non-scandium perovskites recently. In principle, there are plenty of possible new compositions based on BiMeO$_3$–$PbTiO_3$, since B-site Me in BiMeO$_3$ has many combinations and their mean valence is +3 (such as Fe^{3+}, Co^{3+}, $Zn_{1/2}Ti_{1/2}$, or $Ni_{2/3}Nb_{1/3}$). Owing to the metastable nature of the end member of BiMeO$_3$,[9–11] many BiMeO$_3$ compounds exhibit very low solubility within $PbTiO_3$ (less than 10%) under ambient condition, and many $PbTiO_3$–BiMeO$_3$ systems with high solubility of BiMeO$_3$ can only be prepared via unique high-pressure and high-temperature method, such as $xBiCoO_3$–$(1-x)PbTiO_3$, $xBi(Zn_{1/2}Ti_{1/2})O_3$–$(1-x)PbTiO_3$, and $xBi(Zn_{1/2}V_{1/2})O_3$–$(1-x)PbTiO_3$.[12–14]

Notably, thin films can induce internal stresses, which can also stabilize the metastable structures of BiMeO$_3$–$PbTiO_3$ systems, such as $xBi(Zn_{1/2}Ti_{1/2})O_3$–$(1-x)PbTiO_3$.[15] In-

†Corresponding author. E-mail: zhaopan@iphy.ac.cn
‡Corresponding author. E-mail: xmqin@shnu.edu.cn
§Corresponding author. E-mail: ywlong@iphy.ac.cn

© 2024 Chinese Physical Society and IOP Publishing Ltd

deed, the perovskite structure can be well maintained in $0.2Bi(Zn_{1/2}Ti_{1/2})O_3$–$0.8PbTiO_3$ thin film despite its large lattice distortion. In addition, the typical polarization (P) *versus* electrical field (E) loop is successfully observed to be kept in a broad temperature range, but is absent in its bulk state owing to the large leakage current.[15] Favorable ferroelectric performances are also observed in xBi$(Mg_{1/2}Ti_{1/2})O_3$–$(1-x)$PbTiO$_3$ and xBi$(Ni_{1/2}Ti_{1/2})O_3$–$(1-x)$PbTiO$_3$ thin films.[16,17] In addition to the stereochemical $6s^2$, lone-pair electrons in Pb^{2+} and Bi^{3+} have strong hybridizations with oxygen, which is beneficial for ferroelectricity. The strong hybridization between oxygen 2p state and Ti 3d state has an important role in large ferroelectric polarization and enhances ferroelectric-to-paraelectric phase transition temperature of BiMeO$_3$–PbTiO$_3$ system.[18–20] It is therefore considered that Ti ion plays an irreplaceable role in achieving high-performance ferroelectricity. Herein, we design and prepare new Bi-based perovskite thin films $Bi(Cu_{1/2}Ti_{1/2})O_3$–$PbTiO_3$ (hereafter abbreviated as BCT–PT). By using Pt(111)/Ti/SiO_2/Si substrates, we prepare the (100)-oriented BCT–PT thin films. Thereafter, their crystal structures, ferroelectric properties, and fatigue characteristics are studied systematically.

2. Experimental details

The xBi$(Cu_{1/2}Ti_{1/2})O_3$–$(1-x)$PbTiO$_3$ ($x = 0$, 0.1, and 0.2, hereafter abbreviated as xBCT–$(1-x)$PT) precursor solutions were prepared by using titanium n-butoxide [$Ti(OC_4H_9)_4$], lead acetate trihydrate [$Pb(COOCH_3)_2$–$3H_2O$], copper nitrate hemi(pentahydrate) [$Cu(NO_3)_2$–$2.5H_2O$] together with bismuth nitrate pentahydrate [$Bi(NO_3)_3$–$5H_2O$] as raw materials, while 2-methoxyethanol, deionized water, glacial acetic acid and formamide served as solvents, stabilizer, chelator, and surfactant, separately. Continuous stirring under ambient temperature and at atmosphere was required for preparing precursor sol, based on 0.1BCT–0.9PT and 0.2BCT–0.8PT compositions. To make up for component losses caused by annealing, we added 6-mol% Bi and 10-mol% Pb. First of all, 2-methoxyethanol was added to dissolve [$Ti(OC_4H_9)_4$] and [$Pb(COOCH_3)_2$–$3H_2O$]. After that, a small amount of deionized water and glacial acetic acid were successively added into the solution. Then, [$Bi(NO_3)_3$–$5H_2O$] and [$Cu(NO_3)_2$–$2.5H_2O$] were sequentially added into the aforementioned solution under 1-h stirring. Afterwards, to prevent crack appearance, the suitable formamide was further introduced in the resultant solution, followed by 3-h stirring of resulting solution for forming the homogenous BCT–PT precursor solution (0.2 M), as well as another 24-h aging prior to deposition.

To obtain the precursor solution (0.05 M) of PbO seeding layers, [$Pb(COOCH_3)_2$–$3H_2O$] was dissolved in 2-methoxyethanol solvent. For improving crystallinity and (100) preferential orientation of BCT–PT thin film, one PbO layer was deposited with multiple BCT–PT layers in sequence for preparing films. Firstly, we spin-coated PbO seeding layer for a 30-s period at 5000 rpm, and subsequently pyrolyzed it for a 10-min period under 350 °C through using the hot plate, so that it could be deposited onto Pt(111)/Ti/SiO_2/Si substrates. Thereafter, an identical coating and pyrolysis process were adopted to deposit BCT–PT thin films on PbO-coated substrates. These steps were repeated several times to prepare BCT–PT thin film, followed by the deposition of one more PbO seeding layer. By repeating these aforementioned deposition process, a desired thickness ($\sim$ 210 nm) was obtained. Film annealing was conducted for a 40-min period under 700 °C.

The x-ray diffraction patterns (XRD, Smartlab 9 kW and Smartlab, Rigaku, Japan) were employed for analyzing crystallographic microstructure. Additionally, the field emission scanning electron microscopy (FE-SEM, SU8220, Hitachi, Japan) was adopted for examining sample morphologies. The morphology of the as-synthesized samples was characterized by using atomic force microscope (AFM, Bruker Icon). Polarized Raman-scattering data were obtained by using a MonoVista CRS+ 500 spectrometer (Spectroscopy & Imaging, Germany). Ferroelectric, leakage and fatigue characteristics were evaluated with the ferroelectric test system (TF-Analyser 3000, aixACCT, Germany).

3. Results and discussion

Figure 1(a) presents XRD patterns for sol–gel-processed xBCT–$(1-x)$PT ($x = 0$, 0.1, and 0.2) thin films. Clearly, those main peaks of all those investigated thin films are corresponding to the characteristic perovskite structure, with the exception of some diffraction peaks from the substrate. Based on the the longitudinal coordinate of intensity in Fig. 1(a), it can be seen that xBCT–$(1-x)$PT thin films show high stability within the perovskite structure without any noticeable impurities. Note that the (100) diffraction peak intensities in all investigated thin films are much stronger than other peaks, indicating the possible (100) preferential orientation. After fitting the (001) and (100) peaks as shows in Figs. 1(c)–1(e), the relative (100) preferential orientation degrees ($\alpha_{(100)}$) of 0.1BCT–0.9PT ($\alpha_{(100)} = 61.5\%$) and 0.2BCT–0.8PT ($\alpha_{(100)} = 76.5\%$) thin films are estimated by calculating the peak intensity ratio of (100) relative to the sum of (001), (100), (110), and (111), suggesting that the BCT–PT films are predominantly (100) oriented.[21,22] In order to further illustrate the preferred orientation, the different modes of x-ray scanning and pole figure are also performed[23,24] as shown in Fig. 1(b). According to the in-plane XRD and grazing incidence x-ray diffraction (GI-XRD) of 0.1BCT–0.9PT thin films, we not only ob-

served significant changes in peak intensities, but also observed a broadened full width at half maximum (FWHM) of the in-plane mode (100) peak, indicating the presence of (001) peak. In addition, the pole figure showing a ring at $\psi \approx 46^\circ$ corresponds to $\angle(100) : (101) = 46.8^\circ$, which further confirms that the 0.1BCT–0.9PT film is predominantly (100) oriented. The background intensities of the pole figure are in a range of 10 cps–50 cps, while the maximum intensity of the peak at $\psi \approx 46^\circ$ is about 162 cps, and the volume fraction of the $a(b)$-axis-oriented grains is estimated at 30%. Note that in the sol–gel-processed perovskite thin film, it is easier to form simple preferential orientation, such as in the $Bi(Zn_{1/2}Ti_{1/2})O_3$–$PbTiO_3$, $Bi(Mg_{1/2}Ti_{1/2})O_3$–$PbTiO_3$, and $SmFeO_3$–$PbTiO_3$ thin films.[15,16,25]

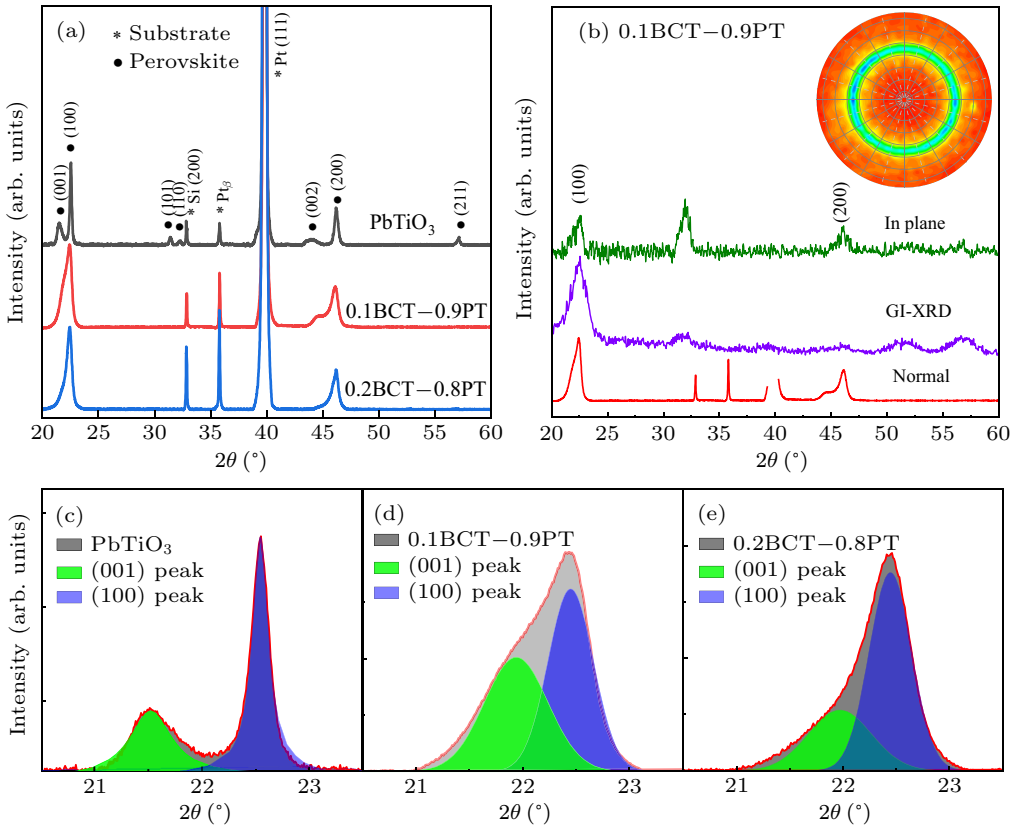


Fig. 1. (a) XRD patterns of xBCT–$(1-x)$PT thin films ($x = 0$, 0.1, and 0.2). (b) In plane XRD pattern and GI-XRD pattern of 0.1BCT–0.9PT thin film, with inset showing x-ray pole figures recorded from 0.1BCT–0.9PT (101) reflection; the rim of the patterns corresponds to $\psi = 75^\circ$. The fitting of (001)/(100) peak of (c) $PbTiO_3$, (d) 0.1BCT–0.9PT, and (e) 0.2BCT–0.8PT.

The evolutions of the lattice distortion (c/a) of xBCT–$(1-x)$PT ($x = 0$, 0.1, and 0.2) thin films can also be observed according to the shift of (100) diffraction peaks in XRD patterns. Here, just one diffraction profile is seen for the {100} tetragonal diffraction index, which slightly shifts to a lower angle, suggesting that a (b) axis increases in thin films. we perform peak fitting of the (001) and (100) diffraction peaks of the xBCT–$(1-x)$PT thin films to different BCT contents, and estimate the axial ratio based on the fitted peak positions. Specifically, the peak positions of the (001) and (100) diffraction peaks in the pure phase $PbTiO_3$ are located at 21.52° and 22.55°, respectively, corresponding to lattice parameters of $a(b) = 3.939$ Å, $c = 4.126$ Å, and $c/a = 1.047$. The 0.1BCT–0.9PT thin film has the fitted lattice parameters $a = 3.957$ Å and $c = 4.048$ Å and the axial ratio $c/a = 1.023$, while the 0.2BCT–0.8PT thin film has the fitted lattice parameters $a = 3.958$ Å and $c = 4.037$ Å, and the axial ratio $c/a = 1.019$. According to the fitting results, it can be seen that the introduction of BCT leads the c axis to decrease and the a axis to increase. As a consequence, it can be observed that c/a decreases with BCT content increasing. The decreasing of c/a indicates the lattice distortion weakening, and therefore promoting the domain switching.[16] Thus, the domain switching in the 0.2BCT–0.8PT thin films is easier than in the 0.1BCT–0.9PT thin films. Notably, c/a ratio of the pristine PT thin film decreases relative to that of PT bulk state, which can be attributed to the size effect and interfacial stress.[26,27] The interfacial stress, which is mainly derived from the thermal expansion mismatch as well as thin film–substrate lattice incomplete relaxation mismatch, would also exist in present xBCT–$(1-x)$PT thin films. It is demonstrated that such a stress is prominent in a-axis domain compared with in the c-axis domain.[26] Therefore, these highly (100) oriented thin films with a greater number of a-axis domains should have a reduced c/a. Similarly, the above result can be obtained from other $BiMeO_3$–$PbTiO_3$ thin films.[16] Notably, in bulk

BiMeO$_3$–PbTiO$_3$ system, some of them have the c/a ratios that do not vary monotonically with BiMeO$_3$ content: c/a ratio increases at lower BiMeO$_3$ content ($< 10\%$), and decreases at higher BiMeO$_3$ content.[28] This is attributed to the competing effects between A-site Pb/Bi-O hybridization and B-site Me/Ti-O hybridization. Generally, the hybridization between Pb/Bi and O is almost unchanged as BiMeO$_3$ level changes, but now it is apparently changed between Me and oxygen. The hybridization between Me and O can descend steeply at high concentration of BiMeO$_3$ when Me has a large cation radius and weak ferroelectric activity.[29]

The cross-sectional and plane view morphologies of 0.2BCT–0.8PT thin films characterized by SEM are shown in Fig. 2(a). The SEM image shows that there are the diverse film layers on the substrate. The surface of the thin film exhibits no cracks or pores, and the thickness of the thin film is about 210 nm. Figures 2(b)–2(d) show the detailed morphologies of the xBCT–$(1-x)$PT ($x = 0, 0.1$, and 0.2) thin films by AFM measurements. According to the AFM images, compared with the pristine PbTiO$_3$ thin films, both 0.1BCT–0.9PT thin film and 0.2BCT–0.8PT thin film show smaller size particles, and their surfaces are smoother. In addition, the distribution of grains in the 0.1BCT–0.9PT and 0.2BCT–0.8PT thin films are more uniform. These would promote the domain switching during measuring the loops of the polarization (P) *versus* the electric field (E).

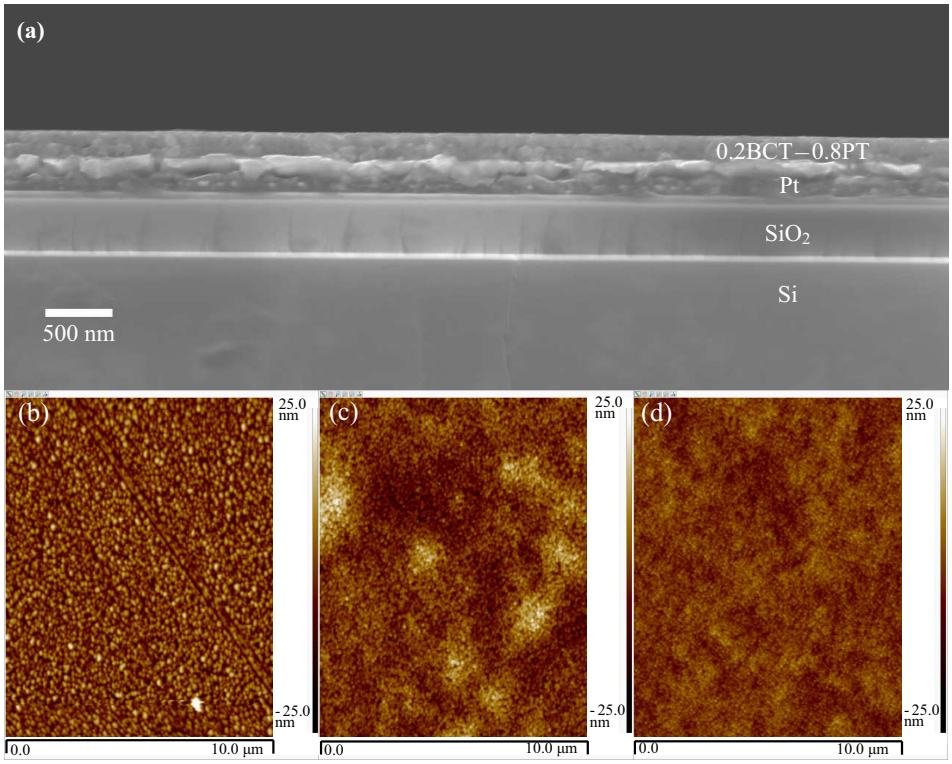


Fig. 2. (a) Cross-sectional SEM image of 0.2BCT–0.8PT thin film, and AFM images of xBCT–$(1-x)$PT thin films for $x = 0$ (b), 0.1 (c), and 0.2 (d).

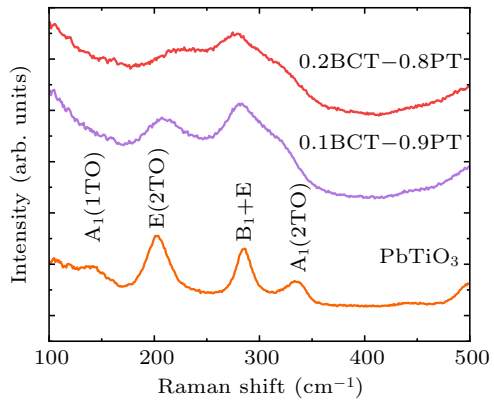


Fig. 3. Raman scattering spectra of BCT–PT films with BCT content of 0, 0.1, and 0.2.

In line with lattice dynamical theory, it is supposed that vibrational soft mode is closely related to spontaneous polarization (P_S) in ferroelectric material. According to the research on lattice dynamics, A$_1$(1TO) soft mode frequently is in direct proportion to order parameter P_S because it represents TiO$_6$ octahedron displacement with respect to Pb atoms.[30] To this end, we investigate the Raman scattering spectra of xBCT–$(1-x)$PT ($x = 0$, 0.1, and 0.2) thin films (Fig. 3). A$_1$(1TO), E(2TO), B1+E, and A$_1$(2TO) peaks can be observed, which correspond to those detected in pristine PT. This indicates that the xBCT–$(1-x)$PT ($x = 0.1$ and 0.2) thin films show the same tetragonal perovskite structure as the pristine PT. Note that the A$_1$(1TO) soft mode shifts towards the lower frequencies as x increases. In addition to A$_1$(1TO), as x increases, A$_1$(2TO) soft mode also shifts towards lower frequencies, and it shows high sensitivity to B-site atom P_S displacement.[30] Based on

these observations, both A_1(1TO) and A_1(2TO) optical modes are softened, accompanied by a reduced c/a. This is consistent with the previous XRD study. Shifts of Raman peaks are associated with the substrate-induced stress effect on thin films. Clearly, non-180° domain wall switching and movement usually leads the value of c/a to be changed significantly. In the present highly (100) oriented xBCT–$(1-x)$PT thin films, non-180° domain instead of the 90° domain is predominant. Therefore, such a reduced c/a promotes switchable ferroelectric domains, and thus enhancing remnant (P_r) and maximal (P_{max}) ferroelectric polarization.[31,32]

Figure 4 displays the P–E loops of xBCT–$(1-x)$PT thin films ($x = 0$, 0.1, and 0.2) under ambient temperature. For the pristine $PbTiO_3$ thin films, the typical P–E loops can be observed only at low electric fields (Fig. 4(a)). Once loading higher electric field, a relative rounded P–E loops appears, indicating the serious leakage current. However, this is not the case in the xBCT–$(1-x)$PT ($x = 0.1$ and 0.2) thin films. It can be seen that each film shows slim P–E loops and high electric endurance, indicating that these thin films are of high quality. Similar slim P–E loops are also observed in PT-based piezoelectric ceramics.[33] $2P_r$ levels of 0.1BCT–0.9PT thin film and 0.2BCT–0.8PT thin film are 30 μC/cm^2 and 16 μC/cm^2, while their coercive field (E_C) values are 126 kV/cm and 115 kV/cm, respectively. With regard to 0.1BCT–0.9PT thin films, their ferroelectric hysteresis loops tend to be saturated as observed from Fig. 4(b). An increased applied electric field can break down the thin films. Therefore, for 0.1BCT–0.9PT thin films, their intrinsic properties are determined when the greatest electric field is applied. With regard to 0.2BCT–0.8PT thin films, a higher electric field can be applied (Fig. 4(c)). However, the P_r value is even smaller than that of the 0.1BCT–0.9PT thin film. These can be explained as follows: the E_C can be the factor indicating the great c/a but low grain size, as observed in PZT thin films.[34] In addition, c/a apparently affects domain switching, such as in typical $BiFeO_3$–$PbTiO_3$-based ceramics, the c/a threshold is determined to be 1.045 in domain switching, while nearly no domain switching happens at the higher value, with inhibiting the new domain from nucleating because of the higher elastic energy inside domain wall.[31] Thus, the introducing of novel domain walls via the electric field becomes difficult in the case of high c/a value. It further indicates that due to the high c/a ratio, the domain switching needs a higher electric field and has a large E_C. Here, 0.1BCT–0.9PT thin films have a larger c/a ratio than 0.2BCT–0.8PT thin films. Correspondingly, domain switching in 0.2BCT–0.8PT thin film can be easier than in 0.1BCT–0.9PT thin film, and a higher electric field can be applied to 0.2BCT–0.8PT thin film. On the other hand, the large c/a can be associated with great P_S displacement, which is the origin of the ferroelectric polarization.[12,35] Hence, the larger polarization values are seen for 0.1BCT–0.9PT thin films than for 0.2BCT–0.8PT thin films.

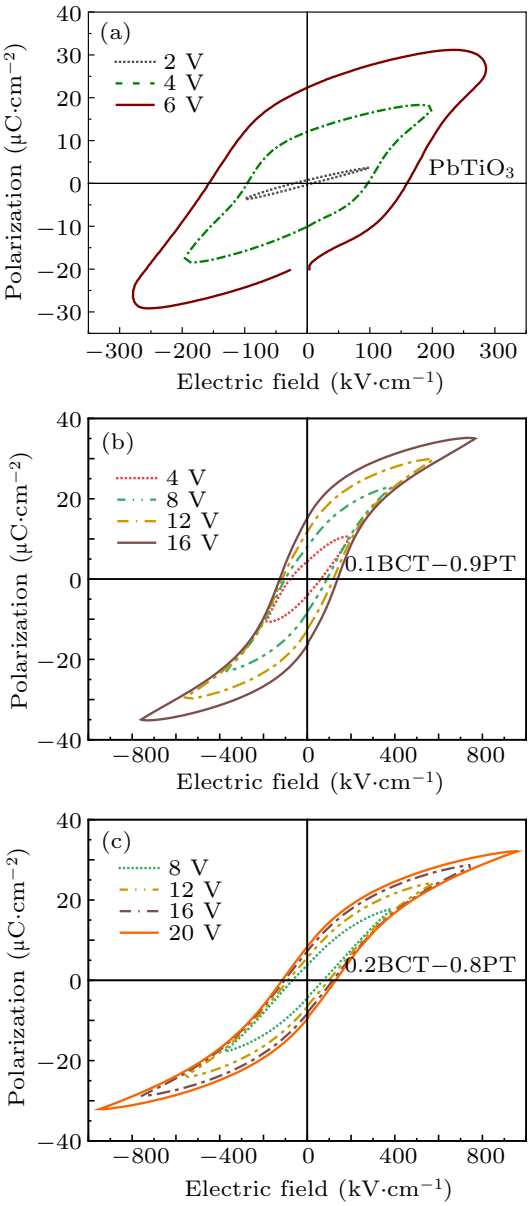


Fig. 4. Ferroelectric hysteresis loops for (a) $PbTiO_3$, (b) 0.1BCT–0.9PT, and (c) 0.2BCT–0.8PT thin films measured at 1 kHz at different applied fields.

To further confirm that the 0.1BCT–0.9PT thin film and 0.2BCT–0.8PT thin film are ferroelectric at room temperature, we carry on measuring the capacitance–voltage (C–V) characteristics of the Pt/xBCT–$(1-x)$PT/Pt ($x = 0.1$ and 0.2) capacitors under a triangular wave at a frequency of 600 mHz as the large signal and a sine wave with a frequency of 1 kHz and amplitude of 25 mV as the small signal. Figure 5 shows the C–V curves of the xBCT–$(1-x)$PT ($x = 0.1$ and 0.2) thin films, indicating a well-defined ferroelectric property for the xBCT–$(1-x)$PT thin films by a butterfly loop behavior. The field corresponding to peak maxima in C–V characteristics is taken

as a coercive field (E_C) and is found to be 130.8 kV/cm and 100.5 kV/cm for 0.1BCT–0.9PT thin film and 0.2BCT–0.8PT thin film, respectively. These values are slightly different from E_C values obtained from *P*–*E* loops, because the *C*–*V* measuring mode is quasi-static while *P*–*E* measurement is dynamic.

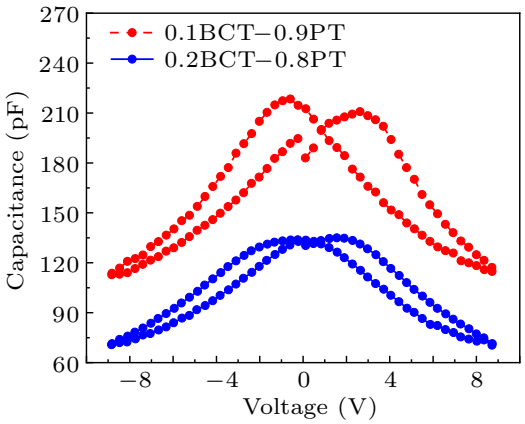


Fig. 5. The *C*–*V* characteristics of xBCT–$(1-x)$PT ($x = 0.1$ and 0.2) thin films.

Figure 6 shows *J*–*E* characteristics of xBCT–$(1-x)$PT ($x = 0.1$ and 0.2) determined under ambient temperature. The pristine $PbTiO_3$ thin films show a very high leakage current of about 1.78×10^{-2} A/cm^2 (Fig. 6(a)). The large leakage current results in the rounded *P*–*E* loops of $PbTiO_3$ thin films during the *P*–*E* loop measurement. Noticeably, unlike the pristine $PbTiO_3$ thin films, the present xBCT–$(1-x)$PT ($x = 0.1$ and 0.2) thin films show relatively low leakage currents. The leakage currents of 0.1BCT–0.9PT thin film and 0.2BCT–0.8PT thin film are 1.64×10^{-4} A/cm^2 and 2.58×10^{-5} A/cm^2, respectively. Note that the smaller leakage current of 0.2BCT–0.8PT thin film allows it to withstand a higher electric field than the 0.1BCT–0.9PT thin film, conforming to $P(E)$ loop measurements. For understanding the reason for charge transport in the above thin film, space charge limited conduction (SCLC) mechanism[36] can be used for explaining the *J*–*E* features, which can be observed from the curves of $\log(J)$ *versus* $\log(E)$ in Fig. 6(b). As can be seen, for the xBCT–$(1-x)$PT ($x = 0$, 0.1, and 0.2) thin films, their slopes from double logarithm *J*–*E* plots approach 1.0 within the low electric field, which demonstrates Ohmic conduction behavior. Moreover, electron content of the transition from the valence band to conduction band by thermionic emission limits the current. The electron content can be deficient under ambient temperature because of the great forbidden ferroelectric gap. Thus, thin films show a lower leakage current in a lower electric field. However, in a high electric region, charge transport is dominated by SCLC mechanism in both the 0.1BCT–0.9PT thin film and 0.2BCT–0.8PT thin film at a ~ 2.0 slope, while the pristine $PbTiO_3$ thin film shows a much larger value. Consistently, herein, J is proportional to E square, namely, $J \propto E^2$.[37] Likewise, the leakage behaviors of other sol–gel deposited Pb-based thin films can also be explained by the similar mechanism.[38,39] It is noteworthy that here 0.1BCT–0.9PT thin film has a slightly larger slope than 0.2BCT–0.8PT thin film in a high electric field, leading to a higher leakage current in the 0.1BCT–0.9PT thin film. This implies that there exist fewer defects in 0.2BCT–0.8PT thin film. Such a result is also consistent with previous $P(E)$ measurement that a higher electric field can be applied to the 0.2BCT–0.8PT thin film than to the 0.1BCT–0.9PT thin film.

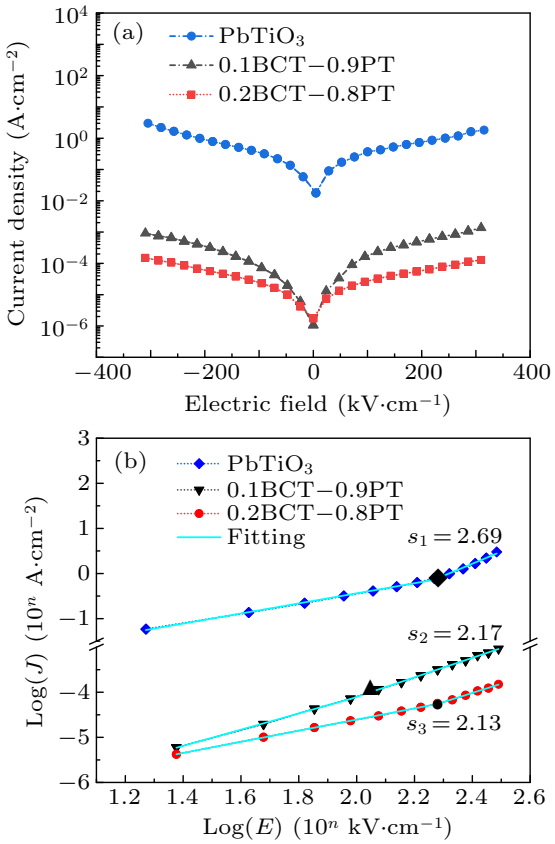


Fig. 6. (a) The *J*–*E* characteristics, and (b) curves of $\log(J)$ *versus* $\log(E)$ of xBCT–$(1-x)$PT thin films ($x = 0$, 0.1, and 0.2) at room temperature.

As far as ferroelectric materials are concerned, the polarization fatigue, the systemic switchable polarization loss in the repetitive bipolar cycling,[40] has been considered to be a major issue restricting applications of ferroelectric thin films in high-quality ferroelectric memories.[41] Switchable polarization is analyzed in the case where the electric field cycling number increases, in order to explore the fatigue process of the present xBCT–$(1-x)$PT ($x = 0$, 0.1, and 0.2) thin films (Fig. 7). To be specific, we analyze a normal electric fatigue process at a measurement pulse frequency of 100 Hz. It can be seen that positive/negative switchable polarization of the xBCT–$(1-x)$PT ($x = 0$, 0.1, and 0.2) thin films decreases with the increase of accumulative cycles. Specifically, for the 0.1BCT–0.9PT thin film, its switchable polarization

decreases by 37.3% of the initial value after about 10^8 cycles, which is lower than the 62.4% initial value of the pristine $PbTiO_3$ thin film after about 10^8 cycles. However, the 0.2BCT–0.8PT thin film shows a more stable fatigue behavior, with the switchable polarization decreasing by 93.6% of initial levels after approximately 10^8 cycles. The present 0.2BCT–0.8PT thin film shows better ferroelectric fatigue properties than the $0.2Bi(Mg_{1/2}Ti_{1/2})O_3$–$0.8PbTiO_3$ thin film, in which the switchable polarization decreases by 45% of its initial value after 10^8 cycles.[16] It also exhibits that the ferroelectric fatigue properties are comparable to the $0.2Bi(Zn_{1/2}Zr_{1/2})O_3$–$0.8PbTiO_3$ thin film.[38] The outstanding fatigue behavior of 0.2BCT–0.8PT thin film is related to its high (100) preferential orientation,[42] uniform and dense structure observed from the XRD and SEM studies, as well as the small leakage current and fewer defects like oxygen vacancies in thin film. In order to better understand the electrical properties of 0.2BCT–0.8PT thin films, we propose the following simple physical process. Under an external electric field, the charge injected into the two poles of the thin film continuously increases, and some of the charges will be captured by some defect centers. In perovskite oxide thin film, oxygen vacancies are the most typical donor type electron capture centers, with energy levels very close to the conduction band. Therefore, after oxygen vacancies capture electrons, their conductivity makes the film exhibit a larger leakage current. Compared with the pristine $PbTiO_3$ thin film, the 0.2BCT–0.8PT thin film shows a smaller leakage current, indicating that the 0.2BCT–0.8PT has fewer defect centers. Furthermore, according to the domain origin model of fatigue in ferroelectric thin films,[43] defect planes that are located parallel to electrodes in the vicinity of the film-electrode interface in the crystal can compensate for the bound charge and elastic stress at the end of the domain by interacting with the domain, thereby pinning the domain system and maintaining fatigue for a long time after the switching process has been terminated. Therefore, the domain pinning behavior of 0.2BCT–0.8PT thin film with fewer charged defect centers is not obvious, o exhibit good fatigue characteristics.

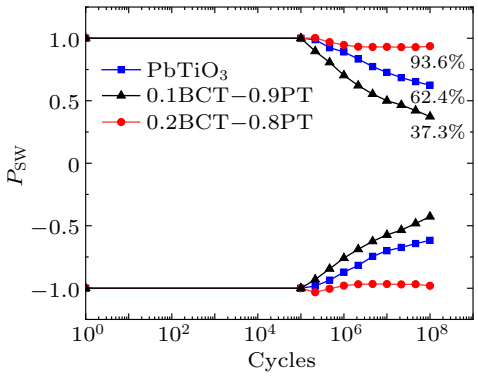


Fig. 7. Plots of normalized switchable polarization *versus* switching cycles for xBCT–$(1-x)$PT thin films ($x = 0$, 0.1, and 0.2).

4. Conclusions

In this work, the sol–gel method is utilized to deposit new Bi-based perovskite thin films based on $Bi(Cu_{1/2}Ti_{1/2})O_3$–$PbTiO_3$, which are 210-nm thick, onto the Pt(111)/Ti/ SiO_2/Si substrates. Related crystal structure, ferroelectric, and fatigue properties are studied systematically. The BCT–PT thin films exhibit great (100) preferential orientation, and the homogeneous and dense microstructure. Moreover, P_r values for 0.1BCT–0.9PT thin film and 0.2BCT–0.8PT thin film are 30 μC/cm^2 and 16 μC/cm^2, respectively. Especially, the 0.2BCT–0.8PT thin film shows the small leakage current and stable polarization fatigue property, which indicates the thin film is suitable for usage in ferroelectric memories.

Acknowledgements

Project supported by the National Key Research and Development Program of China (Grant No. 2021YFA1400300), the National Natural Science Foundation of China (Grant Nos. 22271309, 21805215, 11934017, 12261131499, and 11921004), the Beijing Natural Science Foundation (Grant No. Z200007), and the Fund from the Chinese Academy of Sciences (Grant No. XDB33000000).

References

[1] Damjanovic D 1998 *Rep. Prog. Phys.* **61** 1267
[2] Scott J F 2007 *Science* **315** 954
[3] Wang Y L, Zhao H Q, Zhang L X, Chen J and Xing X R 2017 *Phys. Chem. Chem. Phys.* **19** 17493
[4] Yan Y X, Li Z M, Jin L, Du H L, Zhang M L, Zhang D Y and Hao Y 2021 *ACS Appl. Mater. Interfaces* **13** 38517
[5] Eitel R E, Randall C A, Shrout T R and Park S E 2002 *Jpn. J. Appl. Phys.* **41** 2099
[6] Grinberg I, Suchomel M R, Davies P K and Rappe A M 2005 *J. Appl. Phys.* **98** 094111
[7] Fan L L, Li Q, Zhang L X, Shi N K, Liu H, Ren Y, Chen J and Xing X R 2020 *Inorg. Chem. Front.* **7** 1190
[8] Yoshimura T and Trolier-McKinstry S 2002 *Appl. Phys. Lett.* **81** 2065
[9] Suchomel M R, Fogg A M, Allix M, Niu H, Claridge J B and Rosseinsky M J 2006 *Chem. Mater.* **18** 4987
[10] Belik A A, Wuernisha T, Kamiyama T, Mori K, Maie M, Nagai T, Matsui Y and Takayama-Muromachi E 2006 *Chem. Mater.* **18** 133
[11] Belik A A 2012 *J. Solid State Chem.* **195** 32
[12] Pan Z, Chen J, Yu R Z, *et al*. 2019 *Chem. Mater.* **31** 1296
[13] Pan Z, Jiang X, Chen J, *et al*. 2018 *Inorg. Chem. Front.* **5** 1277
[14] Pan Z, Chen J, Jiang X X, Lin Z S, Zhang H B, Ren Y, Azuma M and Xing X R 2019 *Inorg. Chem. Front.* **6** 1990
[15] Liu L D, Zuo R Z, Sun Q and Liang Q 2013 *J. Sol–Gel Sci. Technol.* **65** 384
[16] Zhang L X, Chen J, Zhao H Q, Fan L L, Rong Y C, Deng J X, Yu R B and Xing X R 2013 *Appl. Phys. Lett.* **103** 082902
[17] Xie Z K, Peng B, Zhang J, Zhang X H, Yue Z X and Li L T 2015 *Ceram. Int.* **41** S206
[18] Cohen R E 1992 *Nature* **358** 136
[19] Kuroiwa Y, Aoyagi S, Sawada A, *et al*. 2001 *Phys. Rev. Lett.* **87** 217601
[20] Yashima M, Omoto K, Chen J, Kato H and Xing X 2001 *Chem. Mater.* **23** 3135
[21] Zhong C F, Wang X H, Wu Y Y and Li L T 2010 *J. Am. Ceram. Soc.* **93** 3993
[22] Cho C R, Lee W J, Yu B G and Kim B W 1999 *J. Appl. Phys.* **86** 2700

[23] Lu C J, Liu X L, Chen X Q, *et al*. 2006 *Appl. Phys. Lett.* **89** 062905
[24] Lu C J, Ye W N, Qi Y J, Liu X L, Senz S and Hesse D 2008 *Phys. Stat. Sol. (a)* **205** 2711
[25] Wang Y L, Zhao H Q, Zhang L X, *et al*. 2016 *Inorg. Chem. Front.* **3** 1473
[26] Lee S H, Jang H M, Cho S M, Yi G C 2002 *Appl. Phys. Lett.* **80** 3165
[27] Akdogan E K, Rawn C J, Porter W D, Payzant E A and Safari A 2005 *J. Appl. Phys.* **97** 084305
[28] Pan Z, Fang Y W, Nishikubo T, Hu L, Kawaguchi S and Azuma M 2022 *Chem. Mater.* **34** 2798
[29] Chen J, Nittala K, Jones J L, Hu P and Xing X 2010 *Appl. Phys. Lett.* **96** 252908
[30] Burns G and Scott B A 1970 *Phys. Rev. Lett.* **25** 167
[31] Chen J, Tan X, Jo W and Rödel J 2009 *J. Appl. Phys.* **106** 034109
[32] Leist T, Granzow T, Jo W and Rödel J 2010 *J. Appl. Phys.* **108** 014103
[33] Cheng M Q, Zhao E D, Jiang F J, *et al*. 2021 *Ceram. Int.* **47** 18417
[34] Liu J S, Zhang S R, Zeng H Z, Yang C T and Yuan Y 2005 *Phys. Rev. B* **72** 172101
[35] Pan Z, Chen J, Fan L L, *et al*. 2017 *Inorg. Chem. Front.* **4** 1352
[36] Lampert M A 1956 *Phys. Rev.* **103** 1648
[37] Khan M A, Comyn T P and Bell A J 2008 *Appl. Phys. Lett.* **92** 072908
[38] Zhang L X, Chen J, Zhao H Q, Fan L L, Rong Y C, Deng J X, Yu R B and Xing X R 2013 *Dalton Trans.* **42** 585
[39] Bai W, Meng X J, Lin T, *et al.* 2009 *J. Appl. Phys.* **106** 124908
[40] Lou X J 2009 *J. Appl. Phys.* **105** 024101
[41] Hannu J, Peräntie J, Stratulat S M, Jantunen H and Tyunina M 2016 *J. Adv. Dielect.* **6** 1650026
[42] Rhun G L, Poullain G, Bouregba R and Leclerc G 2005 *J. Eur. Ceram. Soc.* **25** 2281
[43] Sidorkin A S, Nesterenko L P, Smirnov A L, Smirnov G L, Ryabtsev S V and Sidorkin A A 2008 *Phys. Solid State* **50** 2157